On the Einstein relation between mobility and diffusion coefficient in an active bath

OPEN ACCESS
IOP Publishing
Journal of Physics A: Mathematical and Theoretical
J. Phys. A: Math. Theor. **55** (2022) 184002 (20pp)
https://doi.org/10.1088/1751-8121/ac5d82

On the Einstein relation between mobility and diffusion coefficient in an active bath

Alexandre Solon[1,*] **and Jordan M Horowitz**[2,3,4]

[1] Sorbonne Université, CNRS, Laboratoire de Physique Théorique de la Matière Condensée, LPTMC, F-75005 Paris, France
[2] Department of Biophysics, University of Michigan, Ann Arbor, MI 48109, United States of America
[3] Center for the Study of Complex Systems, University of Michigan, Ann Arbor, MI 48104, United States of America
[4] Department of Physics, University of Michigan, Ann Arbor, MI 48109, United States of America

E-mail: alexandre.solon@sorbonne-universite.fr and jmhorow@umich.edu

Received 27 January 2022, revised 10 March 2022
Accepted for publication 14 March 2022
Published 4 April 2022

Abstract

An active bath, made of self-propelling units, is a nonequilibrium medium in which the Einstein relation $D = \mu k_B T$ between the mobility μ and the diffusivity D of a tracer particle cannot be expected to hold *a priori*. We consider here heavy tracers for which these coefficients can be related to correlation functions which we estimate. We show that, to a good approximation, an Einstein relation does hold in an active bath upon using a different temperature which is defined mechanically, through the pressure exerted on the tracer.

Keywords: active matter, nonequilibrium physics, Stokes–Einstein relation

(Some figures may appear in colour only in the online journal)

Since the seminal experiments of Wu and Libchaber [1], the diffusion of a tracer particle is known to be enhanced when it is placed in an active bath composed of self-propelled entities (bacteria in the experiment). Quantifying this effect is important to understand biological processes such as transport within a cell and to take advantage of the enhanced mixing at the microscopic scale due to the active bath [2, 3]. It has given rise to many experimental [4–12] and theoretical works [13–22]. In the case of bacterial baths, an enhanced diffusivity due to

*Author to whom any correspondence should be addressed.

either direct collisions [11, 13, 20] or far-field hydrodynamic interactions [14–18] has been proposed to account for the experimental measurements.

Whatever the type of interactions, the diffusivity of the tracer is strongly enhanced—e.g. by two orders of magnitude in reference [1]—while its mobility is not affected much. Indeed, most active suspensions are relatively dilute so that the drag force exerted by the active particles is small compared to that exerted by the surrounding fluid. Diffusion and mobility thus have different origins, respectively in the active particles and the surrounding fluid, so that we do not expect them to be related by an Einstein relation as in equilibrium. However, we do expect that if we look at the drag force and noise imparted only by the surrounding fluid, they will be related via the fluctuation–dissipation theorem. Similarly, the active bath imparts drag and noise on the tracer, though their relationship is not as simple since the active bath is out of equilibrium. Multiple methods have been developed to understand the effect of the active bath, for example using modern developments in nonequilibrium linear response theory for weakly interacting tracers [23–25] or by a perturbative analysis of the stochastic equations of motion for soft tracers [26–28]. However, in the experimentally relevant limit of hard, strongly interacting tracers, the effect of an active bath on the diffusion and mobility remains largely unexplored.

With this in mind, we study in this article the effect of an active bath on both diffusion and mobility. To this end, we consider an underdamped tracer subject to passive noise and damping from a surrounding fluid and to the collisions with active Brownian particles (ABPs). We work in the limit of heavy tracers, so that standard projection operator methods [29, 30] allow us to write the noise and damping due to the active bath as fixed-tracer correlation functions, which we evaluate. To highlight similarities and differences, we first consider a bath of passive Brownian particles (PBPs) for which the Einstein relation $D = \mu k_{\mathrm{B}} T$ between the mobility μ and diffusion coefficient D of the tracer directly follows from the Boltzmann distribution. However, an alternate derivation based only on mechanical quantities is possible. From this alternative perspective, the origin of the temperature in the Einstein relation comes from the ideal gas law, where it plays the role of the proportionality constant between pressure and density: $\Pi = \rho_0 k_{\mathrm{B}} T$. In the active case, along similar lines we can introduce a mechanically-defined 'active temperature' T_{a} via the relationship between pressure and density, $T_{\mathrm{a}} = \Pi/(\rho_0 k_{\mathrm{B}})$, where Π is now the mechanical pressure exerted by the active bath on the tracer. We find that, to a good approximation that becomes exact for large tracers, the damping and noise due to the active bath obey an Einstein-like relation involving the active temperature. The full D and μ are then related by a combination of active and passive contributions.

In this study, we consider only spherical tracers. For tracers with a different shape, the physics is expected to be different since they generically induce long-range (power-law decaying) disturbances in an active bath [31, 32]. If the tracer has a polar shape, it will even be spontaneously propelled by the bath, an effect well-established in experiments [33–35]. We work here in two or three spatial dimensions (all simulations are in $d = 2$). Specific effects come into play in $d = 1$ that have been recently explored in references [36, 37].

The paper is organized as follows: in section 1 we introduce the microscopic model. In section 2 we relate the damping and noise due to the bath to correlation functions involving the force on a fixed tracer which we compute in section 3. Finally in section 4 we compute the diffusivity and mobility of the tracer and conclude with a discussion in section 5.

1. The model

We consider a tracer with position and velocity $(\mathbf{R}, \mathbf{V})$ in a bath of either PBPs or ABPs. The ensemble is itself in a surrounding fluid at temperature T that induces a friction of coefficient γ_{T} and γ_{B} on the tracer and bath particles respectively.

The tracer moves according to the Langevin equation

$$m\dot{\mathbf{V}} = \mathbf{F} - \gamma_{\mathrm{T}}\mathbf{V} + \sqrt{2D_{\mathrm{T}}}\boldsymbol{\xi}(t) \tag{1}$$

with Gaussian white noise $\langle \xi_\alpha(t)\xi_\beta(0)\rangle = \delta(t)\delta_{\alpha\beta}$ and $D_{\mathrm{T}} = T\gamma_{\mathrm{T}}$ the noise strength due to the surrounding fluid (here and henceforth we use units such that $k_{\mathrm{B}} = 1$). $\mathbf{F} = \sum_i \mathbf{F}_i$ is the total force imparted by the bath particles, which is the sum of all the forces $\mathbf{F}_i$ due to each particle i.

We assume the bath particles to have an overdamped dynamics. Each bath particle i then follows either one of the two dynamics

$$\dot{\mathbf{r}}_i = -\mu_{\mathrm{B}}\mathbf{F}_i + \mu_{\mathrm{B}}\mathbf{f}_i + \sqrt{2D_{\mathrm{B}}}\boldsymbol{\xi}_i(t), \quad \text{(PBP)} \tag{2}$$

$$\dot{\mathbf{r}}_i = -\mu_{\mathrm{B}}\mathbf{F}_i + \mu_{\mathrm{B}}\mathbf{f}_i + v\mathbf{u}_i, \quad \text{(ABP)}, \tag{3}$$

where $\mathbf{f}_i$ is the force exerted by the other bath particles on particle i. In the passive case, the particle feels a Gaussian white noise with $\langle \xi_{i\alpha}(t)\xi_{j\beta}(0)\rangle = \delta(t)\delta_{\alpha\beta}\delta_{ij}$ and $D_{\mathrm{B}} = \mu_{\mathrm{B}}T$ with $\mu_{\mathrm{B}} = 1/\gamma_{\mathrm{B}}$ while in the active case it is replaced by a self-propulsion at speed v_0 in direction $\mathbf{u}_i$ performing rotational diffusion on the unit sphere. In $d = 2$, this simply reads $\mathbf{u}_i = (\cos\theta_i,\ \sin\theta_i)$ and $\dot{\theta}_i = \sqrt{2D_{\mathrm{r}}}\eta_i(t)$ with η_i a delta-correlated unit-variance Gaussian white noise and D_{r} the rotational diffusion coefficient. Note that in general the rotational diffusion can stem from the active dynamics and thus D_{r} is not related to the temperature.

We consider hardcore interactions between the tracer and bath particles, implemented using the algorithm of reference [38]. On the contrary, among themselves, bath particles interact via a truncated harmonic potential, $\mathbf{f}_i = -\nabla_{r_i}V$ with $V = \sum_{i<j}\frac{k}{2}(\sigma_{\mathrm{B}} - |\mathbf{r}_i - \mathbf{r}_j|)^2$ if $|\mathbf{r}_i - \mathbf{r}_j| < \sigma_{\mathrm{B}}$ and $V = 0$ otherwise. This allows us to vary the bath transport properties by tuning the interaction strength k while we keep the number density $\rho_0 = 1$ fixed. Without loss of generality, we choose the interaction radius of a bath particle $\sigma_{\mathrm{B}} = 1$, thereby fixing the length unit and work in energy units such that $k_{\mathrm{B}} = 1$. The interaction radius between the tracer and the bath particles is denoted σ and is a parameter of the model. We choose the time unit such that $D_{\mathrm{B}} = 1$ for both PBPs and ABPs. In the later case, $D_{\mathrm{B}} = v^2/(2D_{\mathrm{r}}) = vl_{\mathrm{p}}/2$ where $l_{\mathrm{p}} = v/D_{\mathrm{r}}$ is the persistence length. We fix $v = 2$ and $D_{\mathrm{r}} = 0.5$ such that both D_{B} and l_{p} are unity.

2. Effective tracer dynamics

When the motion of the tracer is slow compared to the bath relaxation time, the effect of the bath on the tracer dynamics can be included in an effective equation of motion. To derive this reduced equation for the tracer, we use standard projection operator techniques [29, 30, 39]. Details can be found in appendix A. Here, we outline the main steps, following closely the original exposition for equilibrium fluids [40].

We begin with the Fokker–Planck equation for the probability distribution of the joint position of the tracer in its phase space $(\mathbf{R}, \mathbf{P})$ and the positions of the overdamped Brownian bath particles $\{\mathbf{r}_i\}$ [29],

$$\partial_t P(\mathbf{R}, \mathbf{P}, \mathbf{r}_i) = \mathcal{L}_{\mathrm{T}}P(\mathbf{R}, \mathbf{P}, \mathbf{r}_i) + \mathcal{L}_{\mathrm{B}}P(\mathbf{R}, \mathbf{P}, \mathbf{r}_i), \tag{4}$$

where the Fokker–Planck operators $\mathcal{L}_{\mathrm{T}}$ and $\mathcal{L}_{\mathrm{B}}$ generate the tracer dynamics and the bath dynamics, respectively, in accordance with the Langevin dynamics in equations (1)–(3).

To extract the slow tracer dynamics, we introduce an operator $\mathcal{P}$ that removes the bath ($\mathcal{L}_{\mathrm{B}}\mathcal{P} = \mathcal{P}\mathcal{L}_{\mathrm{B}} = 0$) by projecting the bath onto its steady-state distribution conditioned on the

position of the slow tracer $\pi_{\mathrm{B}}(\mathbf{r}_i|\mathbf{R})$, which is defined as the solution of $\mathcal{L}_{\mathrm{B}}\pi_{\mathrm{B}}(\mathbf{r}_i|\mathbf{R}) = 0$:

$$\mathcal{P}P(\mathbf{R},\mathbf{P},\mathbf{r}_i) = \pi_{\mathrm{B}}(\mathbf{r}_i|\mathbf{R}) \int \prod_i \mathrm{d}\mathbf{r}_i \, P(\mathbf{R},\mathbf{P},\mathbf{r}_i). \tag{5}$$

By applying $\mathcal{P}$ and the orthogonal projector $\mathcal{Q} = \mathcal{I} - \mathcal{P}$ onto the Fokker–Planck equation (4), we arrive at a pair of coupled equations for the relevant $\mathcal{P}P$ and irrelevant $\mathcal{Q}P$ parts of the distribution

$$\partial_t \mathcal{P}P = \mathcal{P}\mathcal{L}_{\mathrm{T}}\mathcal{P}P + \mathcal{P}\mathcal{L}_{\mathrm{T}}\mathcal{Q}P \tag{6}$$

$$\partial_t \mathcal{Q}P = \mathcal{Q}\mathcal{L}_{\mathrm{B}}\mathcal{Q}P + \mathcal{Q}\mathcal{L}_{\mathrm{T}}\mathcal{P}P + \mathcal{Q}\mathcal{L}_{\mathrm{T}}\mathcal{Q}P. \tag{7}$$

Systematically solving for the irrelevant part $\mathcal{Q}P$ assuming that the bath relaxation is fast results in a closed equation for the tracer's evolution,

$$\partial_t \mathcal{P}P = \mathcal{P}\mathcal{L}_{\mathrm{T}}\mathcal{P}P + \mathcal{P}\mathcal{L}_{\mathrm{T}}\mathcal{Q}\int_0^\infty \mathrm{d}s \, \mathrm{e}^{\mathcal{L}_B s}\mathcal{Q}\mathcal{L}_{\mathrm{T}}\mathcal{P}P. \tag{8}$$

The remainder of the derivation requires evaluating each sequence of operators, assuming spherically symmetric particles.

In the end, we find that the effect of the bath can be encapsulated by an additional Gaussian white noise with strength D_{p} and friction γ_{p} (the subscript 'p' stands for 'projected') such that

$$m\dot{\mathbf{V}} = -(\gamma_{\mathrm{T}} + \gamma_{\mathrm{p}})\mathbf{V} + \sqrt{2(D_{\mathrm{T}} + D_{\mathrm{p}})}\boldsymbol{\xi}(t) \tag{9}$$

with coefficients given by the integrals of two-time correlation functions

$$\gamma_{\mathrm{p}} \equiv -\frac{1}{d}\int_0^\infty \langle \mathbf{F}(t) \cdot \nabla \, \log \, \pi_{\mathrm{B}}(0)\rangle_{\mathrm{B}} \, \mathrm{d}t; \qquad D_{\mathrm{p}} \equiv \frac{1}{d}\int_0^\infty \langle \mathbf{F}(t)\cdot\mathbf{F}(0)\rangle_{\mathrm{B}} \, \mathrm{d}t, \tag{10}$$

where $\langle\cdot\rangle_{\mathrm{B}}$ is the average over the bath's steady-state distribution π_{B} with tracer *fixed* at the origin, and d the dimension of space.

To characterize the tracer dynamics we investigate two experimentally-accessible parameters, the mobility μ and the diffusivity D. The mobility is defined as the response to a small constant force (say along the x-axis) $\mathbf{f} = f\mathbf{e}_x$,

$$\mu \equiv \lim_{f\to 0} \frac{\langle V_x\rangle_f}{f}, \tag{11}$$

where $\langle\cdot\rangle_f$ is the steady-state average in presence of the pulling force. The diffusion coefficient is defined as the rate of growth of the mean squared displacement

$$D \equiv \lim_{t\to\infty} \frac{1}{2dt}\langle(\mathbf{R}(t) - \mathbf{R}(0))^2\rangle = \frac{1}{d}\int_0^\infty \langle \mathbf{V}(t)\cdot\mathbf{V}(0)\rangle \mathrm{d}t. \tag{12}$$

For the effective dynamics in equation (9), we can obtain analytic expressions for these quantities. It is first straightforward to show that $\mu = 1/(\gamma_{\mathrm{T}} + \gamma_{\mathrm{p}})$. Furthermore, the steady-state solution of equation (9) is like a Maxwell distribution for the tracer velocity, except with an effective temperature determined by kinematic parameters:

$$\pi_V(\mathbf{V}) \propto \mathrm{e}^{-\frac{mV^2}{2T_{\mathrm{eff}}}}; \qquad T_{\mathrm{eff}} \equiv \frac{D_{\mathrm{T}} + D_{\mathrm{p}}}{\gamma_{\mathrm{T}} + \gamma_{\mathrm{p}}}. \tag{13}$$

An Einstein-like relation then follows from a first-order perturbation theory. Indeed, linear response directly gives that [41]

$$\mu = -\frac{1}{m}\int_0^\infty \left\langle V_x(t)\frac{\partial \pi_V(0)}{\partial V_x}\right\rangle \mathrm{d}t. \tag{14}$$

One then obtains, using the distribution of equation (13),

$$\mu = \beta_{\mathrm{eff}}\int_0^\infty \langle V_x(t)V_x(0)\rangle \mathrm{d}t = D/T_{\mathrm{eff}}, \tag{15}$$

where the last equality follows from the spherical symmetry of the steady state.

All in all, we see that the knowledge of the bath coefficients γ_{p} and D_{p} is enough to compute μ, T_{eff} and thus D from equation (15). To this end, we study in section 3 the correlators that appear in the definitions of γ_{p} and D_{p} before turning to D and μ in section 4.

3. Force autocorrelation

The friction γ_{p} and noise strength D_{p} characterizing the bath, defined in equation (10), are expressed as the time integral of the correlation functions $\langle \mathbf{F}(t)\cdot\nabla \log \pi_{\mathrm{B}}(0)\rangle_{\mathrm{B}}$ and $\langle \mathbf{F}(t)\cdot\mathbf{F}(0)\rangle_{\mathrm{B}}$ respectively.

For a passive bath, one can use the Boltzmann distribution to relate the two correlation functions. Let us denote by V_{HC} the hardcore potential between the tracer and the bath particles. Then using that at equilibrium $\pi_{\mathrm{B}} \propto \mathrm{e}^{-V_{\mathrm{HC}}/T}$, we find that $\nabla \log \pi_{\mathrm{B}} = -\frac{1}{T}\nabla V_{\mathrm{HC}} = \mathbf{F}$ so that the two correlation functions are proportional with a factor T. After integration, one recovers the fluctuation–dissipation theorem $D_{\mathrm{p}} = T\gamma_{\mathrm{p}}$. The implication of this calculation is that to determine the two coefficients, γ_{p} and D_{p}, it is enough to compute the force autocorrelation, which we do in section 3.1.

For active baths, which we discuss in section 3.2, the above reasoning does not hold since the bath particles are not distributed according to the Boltzmann distribution. Nonetheless, for non-interacting active particles, we find that a similar relation holds approximately, $D_{\mathrm{p}} \approx T_{\mathrm{a}}\gamma_{\mathrm{p}}$ with an 'active temperature' T_{a} defined as a mechanical quantity. Again, it is then enough to compute the force autocorrelation, which we do in the limits of small and large tracers compared to the persistence length of the active particles.

3.1. Passive bath

Let us first compute the force autocorrelation $\langle \mathbf{F}(t)\cdot\mathbf{F}(0)\rangle_{\mathrm{B}}$ for non-interacting bath particles. The element of force $\mathbf{dF}$ exerted on a surface element $\mathrm{d}S$ of the tracer around point $\mathbf{r}$ (with the origin at the center of the tracer) is given by the ideal gas law $\mathbf{dF}(0) = -T\rho_{\mathrm{B}}(\mathbf{r})\mathrm{d}S\frac{\mathbf{r}}{|\mathbf{r}|}$ with ρ_{B} the density of bath particles around a fixed tracer. All particles being independent, contributions to the force autocorrelation come about only due to the same particle returning multiple times to the surface. Denoting the transition probability for a single particle in the presence of a tracer of size σ as $P_\sigma(\mathbf{r}', t|\mathbf{r}, 0)$, the element of force exerted at time t on surface $\mathrm{d}S'$ around $\mathbf{r}'$ is again given by the ideal gas law $\mathbf{dF}(t) = -TP_\sigma(\mathbf{r}', t|\mathbf{r}, 0)\mathrm{d}S'\frac{\mathbf{r}'}{|\mathbf{r}'|}$. Integrating over the surface $\mathcal{S}_{\mathrm{T}}$ of the tracer reads

$$\langle \mathbf{F}(t)\cdot\mathbf{F}(0)\rangle_{\mathrm{B}} = \int_{\mathcal{S}_{\mathrm{T}}}\mathrm{d}S'\int_{\mathcal{S}_{\mathrm{T}}}\mathrm{d}S\, T^2\frac{\mathbf{r}\cdot\mathbf{r}'}{|\mathbf{r}||\mathbf{r}'|}P_\sigma(\mathbf{r}', t|\mathbf{r}, 0)\rho_{\mathrm{B}}(\mathbf{r}). \tag{16}$$

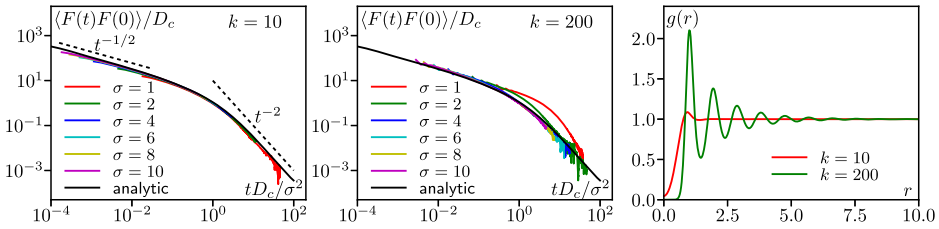

Figure 1. Force autocorrelation for a bath of PBP for varying σ for soft interaction $k = 10$ (left) and harder interaction $k = 200$ (center). Simulations in 2d are compared to the analytic solution equation (20). Right: pair correlation in the fluid showing the increase of the correlation length when k increases. $\rho_0 = 1$, $T = 1$, time step $\mathrm{d}t = 0.003$ and system size 100×100.

Using the spherical symmetry, we can reduce equation (16) to a particle starting on the x-axis at $\mathbf{r} = \sigma \mathbf{e}_x$ and write, using that anywhere outside the tracer $\rho_{\mathrm{B}}(\mathbf{r}) = \rho_0$, the average density,

$$\langle \mathbf{F}(t) \cdot \mathbf{F}(0)\rangle_{\mathrm{B}} = S_{d-1}\sigma^{d-1}\rho_0 T^2 \int_{\mathcal{S}_{\mathrm{T}}} \mathrm{d}S' \cos\theta P_\sigma(\mathbf{r}', t|\sigma \mathbf{e}_x, 0), \tag{17}$$

where θ is the angle between $\mathbf{r}$ and the x-axis and S_d is the solid angle of a d-dimensional sphere so that the area of the tracer is $S_{d-1}\sigma^{d-1}$. Finally, we rescale the length by σ in the integral, and recognize that $P_\sigma(\mathbf{r}'/\sigma, t|\mathbf{e}_x, 0)$ can be replaced by the solution of the diffusion equation around a unit tracer with unit diffusion coefficient, but with diffusively rescaled time $(1/\sigma^d)P_1(\mathbf{r}, tD_{\mathrm{B}}/\sigma|\mathbf{e}_x, 0)$:

$$\langle \mathbf{F}(t) \cdot \mathbf{F}(0)\rangle_{\mathrm{B}} = S_{d-1}\sigma^{d-2}\rho_0 T^2 \int_{\mathcal{S}_{d-1}} \mathrm{d}S' \cos\theta P_1\left(\mathbf{r}', \frac{tD_{\mathrm{B}}}{\sigma^2}|\mathbf{e}_x, 0\right). \tag{18}$$

The integral on the rhs of equation (18) now runs over the solid angle of a sphere $\mathcal{S}_{d-1}$ and is a dimensionless function of the dimensionless time $\tilde{t} = tD_{\mathrm{B}}/\sigma^2$ so that we can write

$$\begin{aligned}\langle \mathbf{F}(t) \cdot \mathbf{F}(0)\rangle_{\mathrm{B}} &= S_{d-1}\sigma^{d-2}\rho_0 T^2 g(tD_{\mathrm{B}}/\sigma^2);\\ g(\tilde{t}) &\equiv \int_{\mathcal{S}_{d-1}} \mathrm{d}S' \cos\theta P_1(\mathbf{r}', \tilde{t}|\mathbf{e}_x, 0).\end{aligned} \tag{19}$$

The function g can be obtained by solving the diffusion equation around the unit sphere. An explicit expression in terms of Bessel functions is obtained for $d = 2$ in appendix B. From figure 1, we see that is displays a power-law behavior $g(\tilde{t}) \sim \tilde{t}^{-1/2}$ at short times crossing over at $\tilde{t} \approx 1$ to $g(\tilde{t}) \sim \tilde{t}^{-2}$.

If the tracer is large enough, the previous calculation also applies straightforwardly to interacting particles, once we recognize that the only hydrodynamic mode in the bath is the density of particles [42]. Indeed, on scales longer than the bath's correlation length and time, the bath's particle density follows the diffusion equation $\partial_t \rho_{\mathrm{B}} = D_{\mathrm{c}}\nabla^2\rho_{\mathrm{B}}$ with a collective diffusion coefficient D_{c}. On this scale, this is a full description of the system, which is thus equivalent to non-interacting particles with a diffusion coefficient D_{c}. One can then repeat the previous derivation, using that the mechanical pressure on the tracer is now $\Pi = D_{\mathrm{c}}\rho_0/\mu_{\mathrm{B}}$ and obtain

$$\langle \mathbf{F}(t) \cdot \mathbf{F}(0)\rangle_{\mathrm{B}} = S_{d-1}\sigma^{d-2}\rho_0 T \frac{D_{\mathrm{c}}}{\mu_{\mathrm{B}}} g\left(\frac{D_{\mathrm{c}}t}{\sigma^2}\right). \tag{20}$$

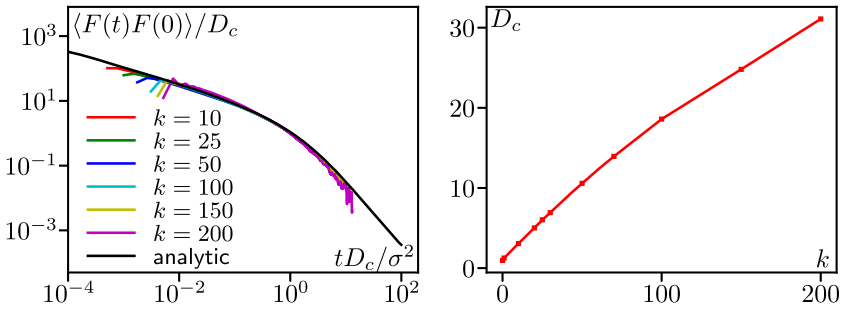

Figure 2. Left: force autocorrelation for a bath of PBP at fixed $\sigma = 6$ for varying interaction strength k showing a good collapse using the collective diffusion D_c. Parameters: $\rho_0 = 1$, $T = 1$, $dt = 0.003$ and system size $L = 100$. Right: $D_c(k)$ measured in relaxation experiments: we start from an inhomogeneous striped initial condition $\rho_B(x) = (1-\alpha)\rho_0$ if $x < L/2$ and $\rho_B(x) = (1+\alpha)\rho_0$ if $x > L/2$ with $\alpha = 0.1$ and extract D_c from the decay of the first Fourier mode $\mathbf{q} = (2\pi/L, 0)$, such that $\hat{\rho}_B(\mathbf{q}, t) \propto e^{-q^2 D_c t}$. Parameters: $L = 100$, $dt = 10^{-3}$, $\rho_0 = 1$.

Compared to equation (19), note that only one of the prefactor T was converted in D_c/μ_B in equation (20). Indeed, following the reasoning that lead to equation (19), the initial element of force $\mathbf{dF}(0)$ is proportional to D_c/μ_B but the one at time t, which corresponds to a single particle returning to the tracer, exerts a pressure proportional to T.

Let us now compare the predictions of equation (20) with results from numerical simulations in 2d. We first look at the effect of the tracer size σ in figure 1 by showing the measured force autocorrelation rescaled as in equation (20) and comparing with the analytic expression obtained for a non-interacting bath. For soft interaction $k = 10$ (left panel), the agreement is excellent. For harder interactions $k = 200$ (center panel), one observes a deviation for small tracers. This is hardly surprising since, as shown in figure 1 (right), pair correlations in the bath extend over a larger distance as k increases. For $k = 200$, we see that correlations extend over $\approx$3 particle radii, consistent with the deviations from scaling, which is expected only when the tracer is larger than the correlation length of the bath.

In figure 2 we vary k at a fixed tracer size $\sigma = 6$, larger than the correlation length for the range of k values tested. We observe an excellent agreement in the whole range. The collective diffusion coefficient D_c used to rescale the curves both in figures 1 and 2 is computed independently in relaxation experiments: starting with an inhomogeneous initial condition (in our case a stripe), the Fourier mode $\mathbf{q}$ of the density field decays as $\hat{\rho}_B(\mathbf{q}, t) \propto e^{-D_c q^2 t}$ which allows us to extract D_c from the rate of exponential decay. The resulting values of D_c are plotted in figure 2 (right). Note that the collective diffusion coefficient increases by a factor of 30 when varying k from 0 to 200 which thus provides a significant test of equation (20). For larger k values, the correlation length diverges rapidly and our theory does not apply anymore.

3.2. Non-interacting active bath

Contrary to the passive case, one cannot resort to the Boltzmann distribution to relate γ_p and the force autocorrelation for active particles. To proceed, let us consider non-interacting particles for which the correlator in γ_p can be written as an integral over the configuration of a single particle (position $\mathbf{r}$ and orientation $\mathbf{u}$) instead of a full microscopic configuration of the bath. This reads

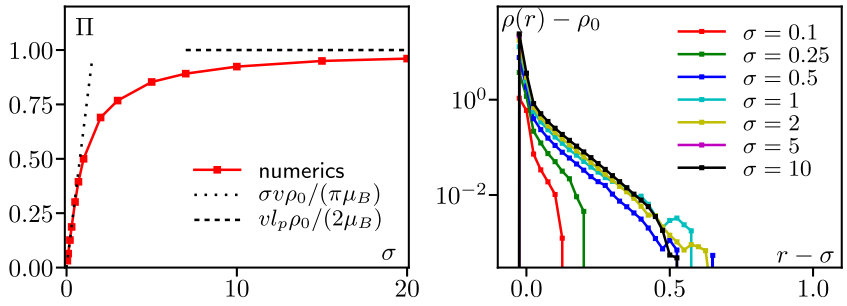

Figure 3. Left: pressure on the tracer due to a bath of non-interacting ABPs as a function of tracer size σ from which the active temperature $T_a = \Pi/\rho_0$ is defined. The dashed and dotted line indicate the two asymptotic regimes considered in the text. Parameters: $v = 2$, $l_r = 1$, $\rho_0 = 1$. $dt = 3 \times 10^{-4}$ and $L = 10$ for $\sigma < 1$. $dt = 3 \times 10^{-3}$ and $L = 60$ for $\sigma > 1$. Right: density profile near the tracer for varying tracer size showing an exponential decay over a small distance. Parameters: $\rho_0 = 1$, $v = 2$, $l_p = 1$, $L = 100$, $dt = 3 \times 10^{-3}$.

$$\langle \mathbf{F}(t) \cdot \nabla \log \pi_B(0) \rangle_B = \int d\mathbf{r} \int d\mathbf{u} \int d\mathbf{r}' \int d\mathbf{u}' \times \left[\mathbf{F}(\mathbf{r}', \mathbf{u}') \cdot \nabla \pi_B(\mathbf{r}, \mathbf{u}) P^A_\sigma(\mathbf{r}', \mathbf{u}', t | \mathbf{r}, \mathbf{u}, 0) \right], \tag{21}$$

where the spatial integrations run over all space and the orientation ones over the unit sphere and $\mathbf{F}(\mathbf{r}', \mathbf{u}')$ is the force exerted on the tracer by a particle at position $\mathbf{r}'$ with orientation $\mathbf{u}'$. We have added a superscript A to the conditional probability P^A_σ to distinguish it from the passive case of section 3.1. To make progress, we can use that, for a hard tracer, $\nabla \pi_B$ is non-zero only close to the surface where the probability distribution $\pi_B(\mathbf{r}, \mathbf{u})$ goes rapidly from 0 inside the tracer to its bulk value ρ_0/S_{d-1} (in the bulk all directions are equiprobable). Although hard to prove rigorously, it is clear numerically, as shown in figure 3 where the density $\rho_B = \int d\mathbf{u}\, \pi_B$ reaches ρ_0 exponentially on a scale smaller than σ. On the contrary, P^A_σ varies smoothly over this range so that we can restrict the integration $\int d\mathbf{r}$ to the surface of the tracer. The integration $\int d\mathbf{r}'$ is also restricted to the surface since $\mathbf{F}(\mathbf{r}', \mathbf{u}')$ vanishes elsewhere. Equation (21) thus simplifies to

$$\langle \mathbf{F}(t) \cdot \nabla \log \pi_B(0) \rangle_B \approx \int_{\mathcal{S}_T} dS \int d\mathbf{u} \int_{\mathcal{S}_T} dS' \int d\mathbf{u}' \times \left[\mathbf{F}(\mathbf{r}', \mathbf{u}') \cdot \left(\frac{\rho_0}{S_{d-1}} \frac{\mathbf{r}}{|\mathbf{r}|} \right) P^A_\sigma(\mathbf{r}', \mathbf{u}', t | \mathbf{r}, \mathbf{u}, 0) \right]. \tag{22}$$

We can now use the ideal gas law to relate equation (22) to the force autocorrelation. The mechanical pressure due to non-interacting active particles is a well-defined, measurable, quantity [43]. Let us then introduce the 'active temperature' T_a such that the pressure on the tracer is $\Pi = T_a \rho_0$. As in section 3.1, the term $-T_a \rho_0 \frac{\mathbf{r}}{|\mathbf{r}|}$ is then the element of force at time $t = 0$ so that equation (22) reduces to the force autocorrelation up to a factor $1/T_a$, i.e.

$$\langle \mathbf{F}(t) \cdot \nabla \log \pi_B(0) \rangle_B \approx \frac{1}{T_a} \langle \mathbf{F}(t) \cdot \mathbf{F}(0) \rangle_B. \tag{23}$$

This implies that $D_p = T_a \gamma_p$ and both can be determined from the force autocorrelation.

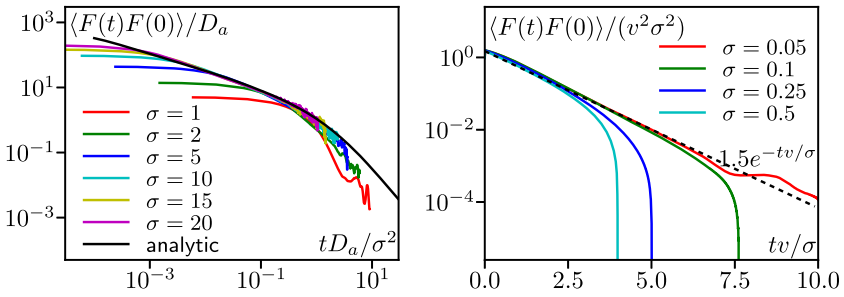

Figure 4. Force autocorrelation for a non-interacting active bath for varying σ. One observes to regimes with different scaling. For large σ (left) the physics is the same as for a passive fluid. The physics at small σ (right), on the contrary, comes purely from the activity. Parameters: $v = 2$, $l_r = 1$. $L = 150$ and $dt = 3 \times 10^{-3}$ (left). $L = 15$ and $dt = 4 \times 10^{-4}$ (right).

Note that the approximation sign in equation (23) comes from the fact that $\nabla\pi_B(\mathbf{r}, \mathbf{u}) \neq 0$ over a finite range near the surface of the tracer. For a passive fluid the dependence in $\mathbf{u}$ disappears and $\nabla\pi_B(\mathbf{r}) = 0$ strictly everywhere except at the surface of the tracer so that equation (23) becomes an equality in the passive case. The temperature entering the fluctuation–dissipation relation $D_p = T\gamma_p$ can thus be seen as coming from the ideal gas law.

In addition to replacing T by T_a, another important difference with the passive case is that the conditional probability $P^A_\sigma(\mathbf{r}', \mathbf{u}', t|\mathbf{r}, \mathbf{u}, 0)$ appearing in the correlators needs to be computed for an ABP instead of a PBP. In general, this is not possible analytically and in the following we look separately at the limits when the tracer is either very large or very small compared to the persistence length of the ABPs.

3.2.1. Large tracer. On time scales larger than the persistence time $\tau_p = D_r^{-1}$, an ABP looses its orientation and is thus effectively diffusing. For large tracers $\sigma \gg l_p$, with $l_p = \nu\tau_p$ the persistence length, the ABP is thus diffusive before it can leave ballistically the tracer (which happens in a time $\sim \sigma/v$). In this case, the motion approaches that of a passive particles and thus $P^A_\sigma = P_\sigma$ (the dependence on $\mathbf{u}'$ and $\mathbf{u}$ in P^A_σ simply becomes irrelevant and can be integrated out). Moreover, as shown in figure 3, the pressure on the tracer approaches that on a flat wall [43], giving $T_a = \frac{v^2}{2D_r\mu_B}$. The force autocorrelation is then the same as in the passive case equation (18) upon replacing T by T_a so that

$$\langle \mathbf{F}(t) \cdot \mathbf{F}(0)\rangle_B = S_{d-1}\sigma^{d-2}\rho_0 T_a^2 g\left(\frac{tD_B}{\sigma^2}\right), \tag{24}$$

where $D_B \equiv \mu_B T_a$ is the bare diffusion coefficient of an ABP.

Figure 4 (left) verifies equation (24) numerically in $d = 2$. One observes that indeed, upon increasing σ, the autocorrelation approaches the same analytical solution as in section 3.1 for a passive bath. The discrepancy at small t is the signature of the finite persistence of the active particles. However, as σ increases, the finite persistence becomes negligible in units of diffusive time σ^2/D_B.

3.2.2. Small tracer. In the opposite limit, when $\sigma \ll l_p$, an ABP initially in contact with the tracer will move far away before changing its orientation. We then expect the relevant time scale to be the ballistic time to leave the tracer σ/v. Moreover, in this regime the active temperature T_a depends on the tracer size $T_a = \frac{v\sigma}{\pi\mu_B}$ in $d = 2$ as shown numerically in figure 3 and reference

[44]. Consistent with this, the scaling that is observed numerically in figure 4 (right) is of the form

$$\langle \mathbf{F}(t) \cdot \mathbf{F}(0) \rangle_{\mathrm{B}} = \sigma^{d-2} T_{\mathrm{a}}^2 \rho_0 h\left(\frac{tv}{\sigma}\right), \tag{25}$$

and we find numerically in $d = 2$ that $h(t) \approx 1.5\,\mathrm{e}^{-t}$. Note that the scalings with σ, both in time and in amplitude (because T_{a} depends on σ) are different from the large-tracer case above.

4. Mobility and diffusivity of the tracer

The coefficients D_{p} and γ_{p} appearing in the effective dynamics of the tracer equation (9) are obtained by time-integrating the force autocorrelation. For the three cases considered in section 3, integrating equations (20), (24) and (25) yield respectively

$$D_{\mathrm{p}} = c\frac{\sigma^d T \rho_0}{\mu_{\mathrm{B}}} = T\gamma_{\mathrm{p}} \qquad \text{(passive)} \tag{26}$$

$$D_{\mathrm{p}} = c\frac{\sigma^d T_{\mathrm{a}} \rho_0}{\mu_{\mathrm{B}}} = T_{\mathrm{a}}\gamma_{\mathrm{p}} \qquad \text{(active)}\, \sigma \gg l_{\mathrm{p}} \tag{27}$$

$$D_{\mathrm{p}} = c'\frac{\sigma^d T_{\mathrm{a}} \rho_0}{\mu_{\mathrm{B}}} = T_{\mathrm{a}}\gamma_{\mathrm{p}} \qquad \text{(active)}\, \sigma \ll l_{\mathrm{p}} \tag{28}$$

with the constants $c = \frac{S_{d-1}}{d}\int_0^\infty g(t)\mathrm{d}t$ and $c' = \frac{\pi}{d}\int_0^\infty h(t)\mathrm{d}t$. The three expressions above are strikingly similar. The differences between these systems are contained in the temperature T or T_{a} (which can depend on σ) and the geometric constant c or c'. In the passive case, the collective diffusion coefficient D_{c} that appears in the force autocorrelation drops out at the integration. The dynamics of the tracer is thus blind to the interactions in the bath.

From there, we can compute the diffusivity and mobility of the tracer from section 2 which gives

$$\mu = \frac{1}{\gamma_{\mathrm{T}} + \gamma_{\mathrm{p}}}; \qquad D = \frac{D_{\mathrm{T}} + D_{\mathrm{p}}}{(\gamma_{\mathrm{T}} + \gamma_{\mathrm{p}})^2}. \tag{29}$$

Let us first consider the case $\gamma_{\mathrm{T}} = 0$, meaning that the surrounding fluid does not affect the tracer. This is probably not the most common situation but provides a good test for the effect of the bath on both μ and D. We show results with $\gamma_{\mathrm{T}} \neq 0$ at the end of this section. For the passive bath or the active bath with $\sigma \gg l_{\mathrm{p}}$, the predictions from equations (26) and (27) are the same

$$\mu = \frac{\mu_{\mathrm{B}}}{c\rho_0\sigma^d}; \qquad D = \frac{D_{\mathrm{B}}}{c\rho_0\sigma^d}. \tag{30}$$

In $d = 2$ we obtain $c = \pi$ (see appendix B). The active case with small tracers $\sigma \ll l_{\mathrm{p}}$ gives

$$\mu = \frac{\mu_{\mathrm{B}}}{c'\rho_0\sigma^d}; \qquad D = \frac{\mu_{\mathrm{B}} T_{\mathrm{a}}}{c'\rho_0\sigma^d}, \tag{31}$$

with $T_{\mathrm{a}} = \sigma\nu/(\pi\mu_{\mathrm{B}})$ and $c' \approx 1.05$ in $d = 2$.

We want to compare our predictions to numerical measurements of D and μ. The mobility is computed from its definition equation (11) by applying a constant external force and measuring the average velocity reached by the tracer. We ensured that we are in the linear regimes by

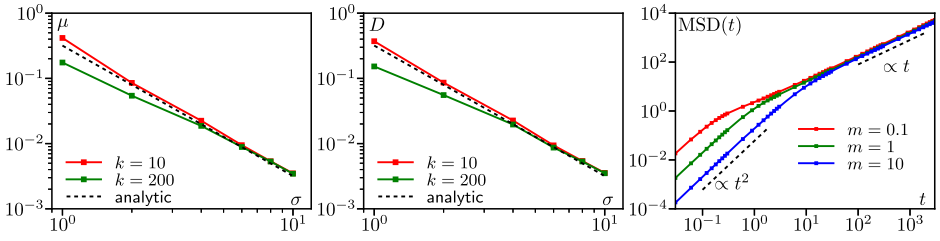

Figure 5. Interacting passive bath. Left: mobility of the tracer measured as the response to a pulling force small enough (here $f = 0.03\sigma^2$) to be in the linear regime. Center: diffusion coefficient measured by fitting the mean-squared displacement of the tracer at late times. Right: mean-squared displacement as a function of mass for three different values of the mass for $k = 10, \sigma = 1$. Parameters: $m = 10$ (except on the right), $L = 100$, $\mathrm{d}t = 3 \times 10^{-3}$.

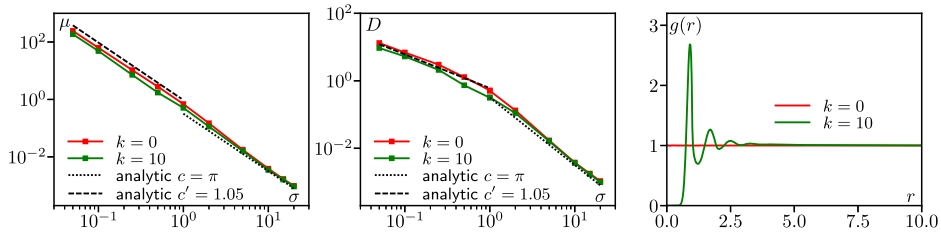

Figure 6. Non-interacting and interacting active baths. Mobility (left) and diffusion coefficient (center) measured as in figure 5. Parameters: $m = 10$ and either $L = 150$, $\mathrm{d}t = 3 \times 10^{-3}$ for $\sigma < 1$ or $L = 15$, $\mathrm{d}t = 3 \times 10^{-4}$ for $\sigma \geqslant 1$. Right: pair correlation in the bath showing that $k = 10$ corresponds to a much higher interaction level than in the passive case (see text).

repeating the measurement for different values of the external force. The diffusivity is fitted on the late-time mean squared displacement of the tracer, in absence of any external force. In measuring D and μ, we make sure that we have reached the limit where the tracer is heavy, the hypothesis used in the calculation of section 2. In practice, as exemplified in figure 5 (right) for the diffusion coefficient, the variation with m is no more than a few percent and we found that using $m = 10$ for all parameters is enough to ensure convergence.

The predictions are compared without any fitting parameter to the numerical simulations in figure 5 for the passive bath and figure 6 for the active one. For the passive bath, the agreement is prefect within numerical accuracy except for the expected deviation for tracers smaller than the correlation length of the bath. In the active case of figure 6 the agreement is again perfect when the tracer becomes large. At small σ, we find a systematic discrepancy of about 25% in the non-interacting case, which can be explained by the approximation made in section 3.2. Nonetheless, the theory captures the correct order of magnitude and, for D, the correct change in behavior with $D \propto \sigma^{-1}$ at small σ and $D \propto \sigma^{-2}$ at large σ.

If the active particles in the bath are interacting, we expect the physics to be more complex since there are three length scales in the system: the tracer size σ, the bath particle size and the persistence length. However, in the limit of large σ, we expect the same argument leading to equation (20) in the passive case to be applicable. Consistently, we observe numerically in figure 6 that the values of D and μ do not depend on the interaction strength k for large σ. For

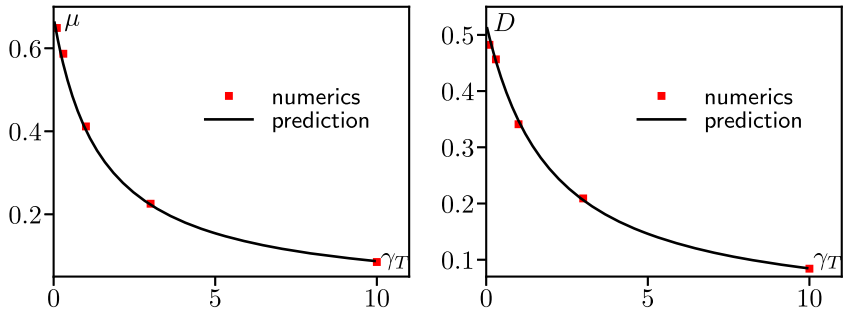

Figure 7. Effect of the external fluid friction with coefficient γ_T on the mobility (left) and diffusivity (right) for a non-interacting active bath and a tracer size $\sigma = 1$. On both panels, the prediction curve is that of equation (29), using the γ_p and D_p measured at $\gamma_T = 0$. Parameters: $k = 0$, $m = 10$, $L = 150$, $dt = 3 \times 10^{-3}$.

smaller σ, their values depend slightly on k but the asymptotic scalings $\mu \propto \sigma^{-2}$ and $D \propto \sigma^{-1}$ are not modified. Note that the value of the interaction strength $k = 10$ corresponds in the active case to a rather strong interaction with several peaks in the pair correlation function, as shown in figure 6 (right) while it was close to the non-interacting limit in the passive case of figure 1. This difference is not surprising. Indeed, for the ballistic motion of ABPs the overlap δ between two particles is of order $\delta \approx v/(\mu_B k)$ while for the diffusive PBPs $\delta \approx \sqrt{T/k}$ so that the active particles become effectively stiffer more rapidly than passive ones as k increases.

Let us finally consider the case when the external fluid acts on the tracer with a coefficient $\gamma_T \neq 0$. This is the most relevant case experimentally since the most common active particles such as bacteria or self-propelled colloids move in a fluid. The mobility and diffusivity of the tracer is then given by equation (29). To verify numerically this formula, we used the values of γ_p and D_p measured when $\gamma_T = 0$ and extrapolate to $\gamma_T \neq 0$ using equation (29). We see in figure 7 that the agreement with direct measurements is perfect up to numerical accuracy.

5. Discussion

In deriving the Einstein relation, our approach based on the effective dynamics of the tracer makes clear that the temperature T appearing in the Einstein relation for a passive bath comes in through the ideal gas law when computing the force autocorrelation in section 3. Although an active bath is not characterized by a single temperature, the mechanical pressure is a perfectly well-defined quantity [43]. This leads us naturally to define an 'active temperature' T_a as the quantity appearing in the ideal gas law and therefore appearing also in the fluctuation–dissipation relation $D_p = T_a \gamma_p$ albeit this is only an approximation in the active case.

When the tracer is subject to both thermal noise and the active bath, the temperatures associated to the two processes do not simply add. Instead the coefficient in the T_{eff} such that $D = \mu T_{eff}$ reads from equation (13)

$$T_{eff} = \frac{T\gamma_T + T_a\gamma_p}{\gamma_T + \gamma_p} \tag{32}$$

which features the damping coefficients due to the fluid and to the bath, respectively γ_T and γ_p. Different regimes are then obtained depending on the parameters. When $\gamma_T \to 0$, as in figure 6,

the fluid does not affect the tracer so that $T_{\rm eff} = T_{\rm a}$. When $\gamma_{\rm T} \gg \gamma_{\rm p}$ but $T_{\rm a}\gamma_{\rm p} \gg T\gamma_{\rm T}$, the damping is controlled by the fluid but the diffusivity comes from the active bath. As discussed in the introduction, this is the regime in which most experiments are performed. One then has $T_{\rm eff} = T_{\rm a}\gamma_{\rm p}/\gamma_{\rm T}$. Ultimately, when $\gamma_{\rm T} \gg \gamma_{\rm p}$ and $T\gamma_{\rm T} \gg T_{\rm a}\gamma_{\rm p}$, we reach a passive limit with $T_{\rm eff} = T$.

Finally, let us remark that for large tracers the values of D and μ appear universal for both passive and active baths. In this limit we obtained

$$\mu = \frac{\mu_{\rm B}}{c\rho_0\sigma^d}; \qquad D = \frac{D_{\rm B}}{c\rho_0\sigma^d}; \tag{33}$$

where the only effect of the bath is through the bare (i.e. single particle) mobility and diffusion coefficient $\mu_{\rm B}$ and $D_{\rm B}$. This is in stark contrast to simple equilibrium fluids, where the Stokes–Einstein relation connects the diffusivity of a large, heavy tracer to the bath's viscosity $D \propto 1/\eta$ (in 3d). While there is no viscosity for Brownian baths as momentum is not conserved and therefore not relevant on hydrodynamic scales, one still might suspect that collective properties of the bath affect a tracer's dynamics. However, we have observed that large tracers are blind to the collective transport properties of the bath, which can be accessed only using tracers that are smaller than the correlation length of a passive bath or the persistence length of an active one. We believe that our understanding of this issue would benefit from a mode-coupling analysis like that carried out in reference [45] to derive the Stokes–Einstein relation from the microscopic Hamiltonian dynamics, where it was shown that one must actually include all higher-order modes to correctly extract the Stokes–Einstein relation.

Note that in this article we have considered only pairwise interaction between bath particles. For active particles, other types of interaction such as quorum-sensing or nonreciprocal ones are possible and more complex phenomena such as flocking and motility-induced phase separation could happen in the bath. The dynamics of a tracer in these complex fluids is an open problem.

Acknowledgments

This work was partially supported by a grant from the Thomas Jefferson Fund, a program of FACE.

Data availability statement

The data that support the findings of this study are available upon reasonable request from the authors.

Appendix A. Derivation of the effective tracer dynamics using projection operators

In this appendix, we review the projection operator technique for extracting the reduced equations for the tracer particle. The methodology is standard [29, 30, 39], with our derivation following closely the original exposition for equilibrium fluids [40].

The probability distribution for the joint position of the tracer in its phase space $(\mathbf{R}, \mathbf{P})$ and the positions of the overdamped Brownian bath particles $\{\mathbf{r}_i\}$ evolves according the Fokker–Planck equation [29]

$$\partial_t P(\mathbf{R}, \mathbf{P}, \mathbf{r}_i) = \mathcal{L}_{\rm T} P(\mathbf{R}, \mathbf{P}, \mathbf{r}_i) + \mathcal{L}_{\rm B} P(\mathbf{R}, \mathbf{P}, \mathbf{r}_i), \tag{A.1}$$

where the tracer dynamics are generated by the Fokker–Planck operator

$$\mathcal{L}_{\mathrm{T}} = -\frac{1}{m}\nabla_{\mathbf{R}}\cdot\mathbf{P} - \nabla_{\mathbf{P}}\left(\mathbf{F} - \frac{\gamma_{\mathrm{T}}}{m}\mathbf{P}\right) + D_{\mathrm{T}}\nabla^2_{\mathbf{P}} \tag{A.2}$$

and the bath dynamics are generated by one of two operators depending on whether they are passive (PBP) or active (ABP)

$$\mathcal{L}_{\mathrm{B}} = \begin{cases} -\mu_{\mathrm{B}}\sum_i \nabla_{\mathbf{r}_i}\cdot(\mathbf{f}_i - \mathbf{F}_i) + D_{\mathrm{B}}\nabla^2_{\mathbf{r}_i} & \text{(PBP)} \\ -\mu_{\mathrm{B}}\sum_i \nabla_{\mathbf{r}_i}\cdot(\mathbf{f}_i - \mathbf{F}_i) - v\nabla_{\mathbf{r}_i}\cdot\mathbf{u}_i + D_{\mathrm{r}}\partial^2_{\theta_i} & \text{(ABP).} \end{cases} \tag{A.3}$$

Within the projection-operator formalism we assume that the bath relaxation time is fast compared to the tracer relaxation time. Thus, we expect that with the tracer fixed, the bath will quickly relax to its steady state distribution conditioned on the position of the tracer $\pi_{\mathrm{B}}(\mathbf{r}_i|\mathbf{R})$ given as the solution of

$$\mathcal{L}_{\mathrm{B}}\pi_{\mathrm{B}}(\mathbf{r}_i|\mathbf{R}) = 0. \tag{A.4}$$

We will assume that this distribution is unique, or, put another way, the null space of $\mathcal{L}_{\mathrm{B}}$ is one dimensional. We will also find it convenient to introduce a notation for steady-state averages with the tracer fixed as $\langle A\rangle_{\mathrm{B}} = \int\prod_i \mathrm{d}\mathbf{r}_i\, A(\mathbf{r}_i)\pi_{\mathrm{B}}(\mathbf{r}_i|\mathbf{R})$.

To exploit this separation of time-scales we introduce a projection operator that projects the bath distribution onto the fixed-tracer steady-state distribution

$$\mathcal{P}P(\mathbf{R},\mathbf{P},\mathbf{r}_i) = \pi_{\mathrm{B}}(\mathbf{r}_i|\mathbf{R})\int\prod_i \mathrm{d}\mathbf{r}_i\, P(\mathbf{R},\mathbf{P},\mathbf{r}_i) \equiv \pi_{\mathrm{B}}(\mathbf{r}_i|\mathbf{R})\rho(\mathbf{R},\mathbf{P}), \tag{A.5}$$

as well as the orthogonal projector $\mathcal{Q} = \mathcal{I} - \mathcal{P}$, where $\mathcal{I}$ is the identity operator. Note, that as is required for a useful projection operator, it projects away the bath dynamics

$$\mathcal{L}_{\mathrm{B}}\mathcal{P} = \mathcal{P}\mathcal{L}_{\mathrm{B}} = 0, \tag{A.6}$$

which can be verified from the definitions of the operators.

We next apply $\mathcal{P}$ and $\mathcal{Q}$ to (A.1) from the left, and insert the identity operator $\mathcal{I} = \mathcal{P} + \mathcal{Q}$ to the right of the Fokker–Planck operators to obtain the pair of equations for the relevant part $\mathcal{P}P$ and irrelevant part $\mathcal{Q}P$,

$$\partial_t\mathcal{P}P = \mathcal{P}\mathcal{L}_{\mathrm{T}}\mathcal{P}P + \mathcal{P}\mathcal{L}_{\mathrm{T}}\mathcal{Q}P \tag{A.7}$$

$$\partial_t\mathcal{Q}P = \mathcal{Q}\mathcal{L}_{\mathrm{B}}\mathcal{Q}P + \mathcal{Q}\mathcal{L}_{\mathrm{T}}\mathcal{P}P + \mathcal{Q}\mathcal{L}_{\mathrm{T}}\mathcal{Q}P, \tag{A.8}$$

where we have suppressed the arguments of the probability distribution to avoid cluttering the equations. Typically at this point one solves the equation for the irrelevant part $\mathcal{Q}P$ formally and substitutes it back into the equation for the relevant part $\mathcal{P}P$ [30]. To obtain a manageable equation, one then typically makes the uncontrolled Markov approximation. Here, we will take a slightly more circuitous route that gives the same results, but has the advantage of making the approximations more clear.

To this end, let us formally introduce a small parameter $\epsilon \ll 1$ into the equation for the irrelevant part $\mathcal{Q}P$ to make explicit the time-scale separation between fast bath and slow tracer dynamics:

$$\partial_t\mathcal{Q}P = \frac{1}{\epsilon}\mathcal{Q}\mathcal{L}_{\mathrm{B}}\mathcal{Q}P + \mathcal{Q}\mathcal{L}_{\mathrm{T}}\mathcal{P}P + \mathcal{Q}\mathcal{L}_{\mathrm{T}}\mathcal{Q}P. \tag{A.9}$$

At the end, we will set $\epsilon = 1$. We can now look for a perturbative solution of the form

$$\mathcal{Q}P = q^{(0)} + \epsilon q^{(1)} + \cdots \tag{A.10}$$

Substituting this into (A.9), we can now solve order by order in ϵ. At lowest order we find

$$\mathcal{Q}\mathcal{L}_{\mathrm{B}} q^{(0)} = (1 - \mathcal{P})\mathcal{L}_{\mathrm{B}} q^{(0)} = \mathcal{L}_{\mathrm{B}} q^{(0)} = 0, \tag{A.11}$$

upon using (A.6). This equation implies that $q^{(0)}$ is in the null space of $\mathcal{L}_{\mathrm{B}}$. However, by definition $\mathcal{Q}P$ is orthogonal to the null space of $\mathcal{L}_{\mathrm{B}}$. Thus, the only solution is $q^{(0)} = 0$. At the next order we have

$$\mathcal{Q}\mathcal{L}_B q^{(1)} + \mathcal{Q}\mathcal{L}_{\mathrm{T}}\mathcal{P}P = 0. \tag{A.12}$$

We can solve this formally, to get the first nontrivial solution for the irrelevant part

$$\mathcal{Q}P \approx q^{(1)} = \mathcal{Q}\int_0^\infty \mathrm{d}s\, \mathrm{e}^{\mathcal{L}_{\mathrm{B}} s}\mathcal{Q}\mathcal{L}_{\mathrm{T}}\mathcal{P}P, \tag{A.13}$$

now setting $\epsilon = 1$ as it is no longer needed.

Having approximated the irrelevant part of the dynamics, we can derive a closed equation for the relevant dynamics by substituting (A.13) into (A.7),

$$\partial_t \mathcal{P}P = \mathcal{P}\mathcal{L}_{\mathrm{T}}\mathcal{P}P + \mathcal{P}\mathcal{L}_{\mathrm{T}}\mathcal{Q}\int_0^\infty \mathrm{d}s\, \mathrm{e}^{\mathcal{L}_B s}\mathcal{Q}\mathcal{L}_{\mathrm{T}}\mathcal{P}P. \tag{A.14}$$

We now turn to evaluating each term using the definitions of the operators. The first term represents the Eulerian part of the dynamics:

$$\mathcal{P}\mathcal{L}_{\mathrm{T}}\mathcal{P}P = \mathcal{P}\left[-\frac{1}{m}\nabla_{\mathbf{R}}\mathbf{P} - \nabla_{\mathbf{P}}\left(\mathbf{F} - \frac{\gamma_{\mathrm{T}}}{m}\mathbf{P}\right) + D_{\mathrm{T}}\nabla_{\mathbf{P}}^2\right]\pi_{\mathrm{B}}\rho \tag{A.15}$$

$$= \mathcal{P}\pi_{\mathrm{B}}\left[-\frac{\mathbf{P}}{m}(\nabla_{\mathbf{R}}\ \ln\ \pi_{\mathrm{B}}) - \frac{1}{m}\nabla_{\mathbf{R}}\mathbf{P} - \nabla_{\mathbf{P}}\left(\mathbf{F} - \frac{\gamma_{\mathrm{T}}}{m}\mathbf{P}\right) + D_{\mathrm{T}}\nabla_{\mathbf{P}}^2\right]\rho \tag{A.16}$$

$$= \pi_{\mathrm{B}}\left[-\frac{\mathbf{P}}{m}\langle\nabla_{\mathbf{R}}\ \ln\ \pi_{\mathrm{B}}\rangle_{\mathrm{B}} - \frac{1}{m}\nabla_{\mathbf{R}}\mathbf{P} - \nabla_{\mathbf{P}}\left(\langle\mathbf{F}\rangle_{\mathrm{B}} - \frac{\gamma_{\mathrm{T}}}{m}\mathbf{P}\right) + D_{\mathrm{T}}\nabla_{\mathbf{P}}^2\right]\rho \tag{A.17}$$

$$= \pi_{\mathrm{B}}\left[-\frac{1}{m}\nabla_{\mathbf{R}}\mathbf{P} + \frac{\gamma_{\mathrm{T}}}{m}\nabla_{\mathbf{P}}\mathbf{P} + D_{\mathrm{T}}\nabla_{\mathbf{P}}^2\right]\rho, \tag{A.18}$$

where in the last line we used the assumed spherical symmetry of the tracer-bath force to set $\langle\mathbf{F}\rangle_{\mathrm{B}} = 0$ and the fact that $\langle\nabla_{\mathbf{R}}\ \ln\ \pi_{\mathrm{B}}\rangle_{\mathrm{B}} = 0$, as π_{B} is normalized. For the second dissipative term we evaluate the effect of the operators one at a time:

$$\mathcal{P}\mathcal{L}_{\mathrm{T}}\mathcal{Q}\,\mathrm{e}^{\mathcal{L}_{\mathrm{B}} s}\mathcal{Q}\mathcal{L}_{\mathrm{T}}\mathcal{P}P \tag{A.19}$$

$$= \mathcal{P}\mathcal{L}_{\mathrm{T}}\mathcal{Q}\,\mathrm{e}^{\mathcal{L}_{\mathrm{B}} s}\mathcal{Q}\pi_{\mathrm{B}}\left[-\frac{\mathbf{P}}{m}\langle\nabla_{\mathbf{R}}\ \ln\ \pi_{\mathrm{B}}\rangle_{\mathrm{B}} - \frac{1}{m}\nabla_{\mathbf{R}}\mathbf{P} - \nabla_{\mathbf{P}}\left(\langle\mathbf{F}\rangle_{\mathrm{B}} - \frac{\gamma_{\mathrm{T}}}{m}\mathbf{P}\right) + D_{\mathrm{T}}\nabla_{\mathbf{P}}^2\right]\rho \tag{A.20}$$

$$= \mathcal{P}\mathcal{L}_{\mathrm{T}}\mathcal{Q}\, \mathrm{e}^{\mathcal{L}_{\mathrm{B}} s}\pi_{\mathrm{B}} \left[-\frac{\mathbf{P}}{m}(\nabla_{\mathbf{R}} \ln \pi_{\mathrm{B}}) - \nabla_{\mathbf{P}}\mathbf{F}\right] \rho \tag{A.21}$$

$$= \mathcal{P}\mathcal{L}_{T}\, \mathrm{e}^{\mathcal{L}_{\mathrm{B}} s}\pi_{\mathrm{B}} \left[-\frac{\mathbf{P}}{m}(\nabla_{\mathbf{R}} \ln \pi_{\mathrm{B}}) - \nabla_{\mathbf{P}}\mathbf{F}\right] \rho \tag{A.22}$$

$$= \mathcal{P}\left[-\frac{1}{m}\nabla_{\mathbf{R}}\mathbf{P} - \nabla_{\mathbf{P}}\left(\mathbf{F} - \frac{\gamma_{\mathrm{T}}}{m}\mathbf{P}\right) + D_{\mathrm{T}}\nabla_{\mathbf{P}}^2\right] \mathrm{e}^{\mathcal{L}_{\mathrm{B}} s}\pi_{\mathrm{B}}$$
$$\times \left[-\frac{\mathbf{P}}{m}(\nabla_{\mathbf{R}} \ln \pi_{\mathrm{B}}) - \nabla_{\mathbf{P}}\mathbf{F}\right] \rho \tag{A.23}$$

$$= \pi_{\mathrm{B}}\left[\nabla_{\mathbf{P}}\left\langle \mathbf{F}\, \mathrm{e}^{\mathcal{L}_{\mathrm{B}} s}\nabla_{\mathbf{R}} \ln \pi_{\mathrm{B}}\right\rangle_{\mathrm{B}}\frac{\mathbf{P}}{m} + \nabla_{\mathbf{P}}\left\langle \mathbf{F}\, \mathrm{e}^{\mathcal{L}_{\mathrm{B}} s}\mathbf{F}\right\rangle_{\mathrm{B}}\nabla_{\mathbf{P}}\right] \rho. \tag{A.24}$$

Thus,

$$\mathcal{P}\mathcal{L}_{\mathrm{T}}\mathcal{Q}\int_0^\infty \mathrm{d}s\, \mathrm{e}^{\mathcal{L}_{\mathrm{B}} s}\mathcal{Q}\mathcal{L}_{\mathrm{T}}\mathcal{P}P = \pi_{\mathrm{B}}\left[\nabla_{\mathbf{P}}\cdot\hat{\gamma}_{\mathrm{p}}\cdot\frac{\mathbf{P}}{m} + \nabla_{\mathbf{P}}\cdot\hat{D}_{\mathrm{p}}\cdot\nabla_{\mathbf{P}}\right]\rho, \tag{A.25}$$

having identified

$$\hat{\gamma}_{\mathrm{p}} = \int_0^\infty \left\langle \mathbf{F}\, \mathrm{e}^{\mathcal{L}_{\mathrm{B}} s}\nabla_{\mathbf{R}} \ln \pi_{\mathrm{B}}\right\rangle_{\mathrm{B}}\mathrm{d}s = \int_0^\infty \langle \mathbf{F}(s)\nabla_{\mathbf{R}} \ln \pi_{\mathrm{B}}(0)\rangle_B \mathrm{d}s \tag{A.26}$$

$$\hat{D}_{\mathrm{p}} = \int_0^\infty \left\langle \mathbf{F}\, \mathrm{e}^{\mathcal{L}_{\mathrm{B}} s}\mathbf{F}\right\rangle_{\mathrm{B}}\mathrm{d}s = \int_0^\infty \langle \mathbf{F}(s)\mathbf{F}(0)\rangle_{\mathrm{B}}\mathrm{d}s, \tag{A.27}$$

which we recognize as operator representations of steady-state correlation functions. These expressions can be simplified using spherical symmetry to conclude that they are both proportional to the identify $\hat{\gamma}_{\mathrm{p}} = \gamma_{\mathrm{p}}\hat{I}$ and $\hat{D}_{\mathrm{p}} = D_{\mathrm{p}}\hat{I}$ and by replacing $\nabla_{\mathbf{R}} \to -\nabla$ due to the translational invariance of the bath steady state, thereby arriving at (10).

Finally, putting everything together, we find a closed equation for the tracer dynamics

$$\partial_t\rho = \left[-\frac{1}{m}\nabla_{\mathbf{R}}\mathbf{P} + \frac{\gamma_{\mathrm{T}} + \gamma_{\mathrm{P}}}{m}\nabla_{\mathbf{P}}\cdot\mathbf{P} + (D_{\mathrm{T}} + D_{\mathrm{p}})\nabla_{\mathbf{P}}^2\right]\rho, \tag{A.28}$$

where the equivalent Langevin equation is used in (9).

Appendix B. Exact force–force correlation for a passive particle in 2D

In this appendix, we solve the 2D diffusion equation around a disk in order to find an explicit expression for $g(t)$ (19), which captures the time-dependence of the correlation function of the force on the tracer due to a bath of independent PBPs.

Determining the force correlation function is equivalent to finding the Green's function for a Brownian particle diffusing in an annulus of inner radius σ and outer radius L. For large L, the shape of the region should be immaterial, allowing us to compare the results of this analytical calculation to the simulations. Denoting the position of the particle as (r, θ) in polar coordinates, we obtain the Green's function as the solution of the diffusion equation for the time-dependent probability distribution $P(r, \theta, t)$,

$$\partial_t P(r,\theta,t) = \nabla^2 P(r,\theta,t) = \frac{1}{r}\partial_r\left[r\partial_r P(r,\theta,t)\right] + \frac{1}{r^2}\partial_\theta^2 P(r,\theta,t), \tag{B.1}$$

with delta-function initial condition at the point (r_0, θ_0) and no flux boundary conditions,

$$P(r,\theta,0) = \delta(r-r_0)\delta(\theta-\theta_0)/r_0 \tag{B.2}$$

$$\partial_r P(\sigma,\theta,t) = \partial_r P(L,\theta,t) = 0, \qquad P(r,0,t) = P(r,2\pi,t). \tag{B.3}$$

The solution can be obtained using an eigendecomposition

$$P(r,\theta,t) = \sum_\lambda \mathrm{e}^{-\lambda t} f_\lambda(r,\theta) f_\lambda(r_0,\theta_0), \tag{B.4}$$

where the eigenfunctions f_λ satisfy

$$-\lambda f(r,\theta) = \frac{1}{r}\partial_r\left[r\partial_r f(r,\theta)\right] + \frac{1}{r^2}\partial_\theta^2 f(r,\theta). \tag{B.5}$$

While the solution is well known in general, imposing the no-flux boundary conditions requires some delicate analysis, so we review the solution here.

To proceed we look for separable solutions $f_\lambda(r,\theta) = R(r)\Theta(\theta)$. Substituting this ansatz into (B.5), we find that the pair of functions R and Θ must satisfy

$$\partial_\theta^2\Theta(\theta) + l^2\Theta(\theta) = 0 \tag{B.6}$$

$$r^2\partial_r^2 R(r) + r\partial_r R(r) + \left(\lambda r^2 - l^2\right) R(r)^2 = 0, \tag{B.7}$$

where the constants λ and l are fixed by the boundary conditions. To satisfy the periodic boundary condition, $\Theta(0) = \Theta(2\pi)$, we find that $l = n$ with $n \in \mathbb{N}$ and then (B.6) has two possible solutions

$$\Theta(\theta) = \begin{cases} \cos(n\theta) \\ \sin(n\theta), \end{cases} \tag{B.8}$$

when $n \neq 0$ and is simply $\Theta(\theta) = 1$ when $n = 0$.

With $l = n$ an integer, we recognize that (B.7) is Bessel's equation, whose solution can be written in terms of nth order Bessel functions of the first J_n and second Y_n kind,

$$R(r) = AJ_n(\sqrt{\lambda}r) + BY_n(\sqrt{\lambda}r), \tag{B.9}$$

where the constants A and B are fixed by imposing the no-flux boundary conditions ($\partial_r R(\sigma) = \partial_r R(L) = 0$):

$$AJ_n'(\sqrt{\lambda}\sigma) + BY_n'(\sqrt{\lambda}\sigma) = 0 \tag{B.10}$$

$$AJ_n'(\sqrt{\lambda}L) + BY_n'(\sqrt{\lambda}L) = 0. \tag{B.11}$$

To have nontrivial solutions for A and B the two equations must be linearly dependent, which will only be true when the determinant vanishes,

$$\begin{vmatrix} J_n'(\sqrt{\lambda}\sigma) & Y_n'(\sqrt{\lambda}\sigma) \\ J_n'(\sqrt{\lambda}L) & Y_n'(\sqrt{\lambda}L) \end{vmatrix} = J_n'(\sqrt{\lambda}\sigma)Y_n'(\sqrt{\lambda}L) - J_n'(\sqrt{\lambda}L)Y_n'(\sqrt{\lambda}\sigma) = 0. \tag{B.12}$$

This is the required condition to fix the eigenvalues λ. To exploit this, let us define the zeros α_{nm} of the determinant equation as

$$J_n'(\alpha_{nm}\sigma)Y_n'(\alpha_{nm}L) - J_n'(\alpha_{nm}L)Y_n'(\alpha_{nm}\sigma) = 0. \tag{B.13}$$

Then the eigenvalues are $\lambda = \alpha_{nm}^2$, and our solution becomes

$$R(r) = AJ_n(\alpha_{nm}r) + BY_n(\alpha_{nm}r). \tag{B.14}$$

We can now fix one of the constants using either of the boundary conditions (B.10) and (B.11), as they are now linearly dependent. The radial component of the eigenfunction is then

$$R_{nm}(r) = J_n(\alpha_{nm}r)Y_n'(\alpha_{nm}L) - Y_n(\alpha_{nm}r)J_n'(\alpha_{nm}L), \tag{B.15}$$

as long $n > 0$ and $m > 0$. However, when $n = 0$, then $\lambda = 0$ is a possible solution. In this case, $R_{00}(r) = 1$.

Putting it all together and normalizing, we find for our eigenfunctions

$$f_{nm}(r,\theta) = \frac{1}{\pi N_{nm}} R_{nm}(r) \times \begin{cases} \cos(n\theta) \\ \sin(n\theta) \end{cases} \quad n, m \geqslant 1 \tag{B.16}$$

$$f_{0m}(r,\theta) = \frac{1}{2\pi N_{0m}} R_{0m}(r), \qquad n = 0,\ m \geqslant 1 \tag{B.17}$$

$$f_{00}(r,\theta) = \frac{1}{\pi(L^2 - \sigma^2)}, \qquad n = m = 0, \tag{B.18}$$

where we have introduced the normalization $N_{nm} = \int_\sigma^L R_{nm}(r)^2 r\,\mathrm{d}r$. Substituting into (B.4), we arrive at our final expression for the Green's function

$$P(r,\theta,t|r_0,\theta_0,0) = \frac{1}{\pi(L^2 - a^2)} + \frac{1}{2\pi}\sum_{m\geqslant 1} \mathrm{e}^{-\alpha_{0m}^2 t} \frac{R_{0m}(r)R_{0m}(r_0)}{N_{0m}} \tag{B.19}$$

$$+ \frac{1}{\pi}\sum_{n,m\geqslant 1} \mathrm{e}^{-\alpha_{nm}^2 t} \frac{R_{nm}(r)R_{nm}(r_0)}{N_{nm}} \left(\cos(n\theta)\cos(n\theta_0)\right. \\ \left. + \sin(n\theta)\sin(n\theta_0)\right). \tag{B.20}$$

With the Green's function in hand, all that is left is to obtain $g(t)$ is to evaluate the integral in (19) for a tracer of radius $\sigma = 1$ in two dimensions,

$$g(t) = \int_0^{2\pi} \cos(\theta) P(1,\theta,t|1,0,0)\mathrm{d}\theta. \tag{B.21}$$

We observe that $\cos(\theta)$ is orthogonal to every eigenfunction except when $n = 1$. As a result,

$$g(t) = \sum_{m\geqslant 1} \mathrm{e}^{-\alpha_{1m}^2 t} \frac{R_{1m}(1)^2}{N_{1m}}. \tag{B.22}$$

Data in figures were generated by numerically approximating this sum using the first 1000 nonzero eigenvalues for parameter values $\sigma = 1$ and $L = 25$.

ORCID iDs

Alexandre Solon https://orcid.org/0000-0002-0222-1347
Jordan M Horowitz https://orcid.org/0000-0002-9139-0811

References

[1] Wu X-L and Libchaber A 2000 Particle diffusion in a quasi-two-dimensional bacterial bath *Phys. Rev. Lett.* **84** 3017
[2] Kim M J and Breuer K S 2007 Controlled mixing in microfluidic systems using bacterial chemotaxis *Anal. Chem.* **79** 955–9
[3] Belan S and Kardar M 2019 Pair dispersion in dilute suspension of active swimmers *J. Chem. Phys.* **150** 064907
[4] Chen D T N, Lau A W C, Hough L A, Islam M F, Goulian M, Lubensky T C and Yodh A G 2007 Fluctuations and rheology in active bacterial suspensions *Phys. Rev. Lett.* **99** 148302
[5] Leptos K C, Guasto J S, Gollub J P, Pesci A I and Goldstein R E 2009 Dynamics of enhanced tracer diffusion in suspensions of swimming eukaryotic microorganisms *Phys. Rev. Lett.* **103** 198103
[6] Valeriani C, Li M, Novosel J, Arlt J and Marenduzzo D 2011 Colloids in a bacterial bath: simulations and experiments *Soft Matter* **7** 5228–38
[7] Mino G *et al* 2011 Enhanced diffusion due to active swimmers at a solid surface *Phys. Rev. Lett.* **106** 048102
[8] Jeanneret R, Pushkin D O, Kantsler V and Polin M 2016 Entrainment dominates the interaction of microalgae with micron-sized objects *Nat. Commun.* **7** 1–7
[9] Maggi C, Paoluzzi M, Angelani L and Di Leonardo R 2017 Memory-less response and violation of the fluctuation–dissipation theorem in colloids suspended in an active bath *Sci. Rep.* **7** 1–7
[10] Ortlieb L, Rafaï S, Peyla P, Wagner C and John T 2019 Statistics of colloidal suspensions stirred by microswimmers *Phys. Rev. Lett.* **122** 148101
[11] Lagarde A, Dagès N, Nemoto T, Démery V, Bartolo D and Gibaud T 2020 Colloidal transport in bacteria suspensions: from bacteria collision to anomalous and enhanced diffusion *Soft Matter* **16** 7503–12
[12] Seyforth H, Gomez M, Rogers W B, Ross J L and Ahmed W W 2021 Non-equilibrium fluctuations and nonlinear response of an active bath (arXiv:2110.15917)
[13] Squires T M and Brady J F 2005 A simple paradigm for active and nonlinear microrheology *Phys. Fluids* **17** 073101
[14] Underhill P T, Hernandez-Ortiz J P and Graham M D 2008 Diffusion and spatial correlations in suspensions of swimming particles *Phys. Rev. Lett.* **100** 248101
[15] Lin Z, Thiffeault J-L and Childress S 2011 Stirring by squirmers *J. Fluid Mech.* **669** 167–77
[16] Pushkin D O and Yeomans J M 2013 Fluid mixing by curved trajectories of microswimmers *Phys. Rev. Lett.* **111** 188101
[17] Morozov A and Marenduzzo D 2014 Enhanced diffusion of tracer particles in dilute bacterial suspensions *Soft Matter* **10** 2748–58
[18] Thiffeault J-L 2015 Distribution of particle displacements due to swimming microorganisms *Phys. Rev.* E **92** 023023
[19] Reichhardt C and Reichhardt C J O 2015 Active microrheology in active matter systems: mobility, intermittency, and avalanches *Phys. Rev.* E **91** 032313
[20] Burkholder E W and Brady J F 2017 Tracer diffusion in active suspensions *Phys. Rev.* E **95** 052605
[21] Dal Cengio S, Levis D and Pagonabarraga I 2019 Linear response theory and Green–Kubo relations for active matter *Phys. Rev. Lett.* **123** 238003
[22] Knežević M, Podgurski L E A and Stark H 2021 Oscillatory active microrheology of active suspensions *Sci. Rep.* **11** 1–10
[23] Maes C 2014 On the second fluctuation–dissipation theorem for nonequilibrium baths *J. Stat. Phys.* **154** 705–22
[24] Steffenoni S, Kory K and Galasco G 2016 Interacting Brownian dynamics in a nonequilibrium particle bath *Phys. Rev.* E **94** 062139
[25] Maes C 2020 Fluctuating motion in an active environment *Phys. Rev. Lett.* **125** 208001
[26] Démery V, Bénichou O and Jacquin H 2014 Generalized Langevin equations for a driven tracer in dense soft colloids: construction and applications *New J. Phys.* **16** 053032

[27] Démery V and Fodor É 2019 Driven probe under harmonic confinement in a colloidal bath *J. Stat. Mech.* 033202
[28] Feng M and Hou Z 2021 Effective dynamics of tracer in active bath: a mean-field theory study (arXiv:2110.00279)
[29] Gardiner C 2009 *Stochastic Methods: A Handbook for the Natural and Social Sciences* (*Springer Series in Synergetics*) (Berlin: Springer)
[30] Zwanzig R 2001 *Nonequilibrium Statistical Mechanics* (New York: Oxford University Press)
[31] Baek Y, Solon A P, Xu X, Nikola N and Kafri Y 2018 Generic long-range interactions between passive bodies in an active fluid *Phys. Rev. Lett.* **120** 058002
[32] Granek O, Baek Y, Kafri Y and Solon A P 2020 Bodies in an interacting active fluid: far-field influence of a single body and interaction between two bodies *J. Stat. Mech.* 063211
[33] Di Leonardo R *et al* 2010 Bacterial ratchet motors *Proc. Natl Acad. Sci. USA* **107** 9541–5
[34] Sokolov A, Apodaca M M, Grzybowski B A and Aranson I S 2010 Swimming bacteria power microscopic gears *Proc. Natl Acad. Sci. USA* **107** 969–74
[35] Kaiser A, Peshkov A, Sokolov A, ten Hagen B, Löwen H and Aranson I S 2014 Transport powered by bacterial turbulence *Phys. Rev. Lett.* **112** 158101
[36] Banerjee T, Jack R L and Cates M E 2021 Tracer dynamics in one dimensional gases of active or passive particles (arXiv:2109.10188)
[37] Granek O, Kafri Y and Tailleur J 2021 The anomalous transport of tracers in active baths (arXiv:2108.11970)
[38] Scala A, Voigtmann T and De Michele C 2007 Event-driven Brownian dynamics for hard spheres *J. Chem. Phys.* **126** 134109
[39] Espanõl P 2002 Coarse graining from coarse-grained descriptions *Phil. Trans. R. Soc.* A **360** 383–94
[40] Van Kampen N G and Oppenheim I 1986 Brownian motion as a problem of eliminating fast variables *Physica*A **138** 231–48
[41] Risken H 1996 Fokker–Planck equation *The Fokker–Planck Equation* (Berlin: Springer) pp 63–95
[42] Hess W and Klein R 1983 Generalized hydrodynamics of systems of Brownian particles *Adv. Phys.* **32** 173–283
[43] Solon A P, Fily Y, Baskaran A, Cates M E, Kafri Y, Kardar M and Tailleur J 2015 Pressure is not a state function for generic active fluids *Nat. Phys.* **11** 673–8
[44] Smallenburg F and Löwen H 2015 Swim pressure on walls with curves and corners *Phys. Rev.* E **92** 032304
[45] Schofield J and Oppenheim I 1992 Mode coupling and tagged particle correlation functions: the Stokes–Einstein law *Physica*A **187** 210–42